Original Article

Experimental investigation of formability and surface quality of tinplate sheets in the single-point incremental forming process

Rafael Oliveira Santos [1,2*]
Victor Gabriel Pereira Ramos [2]
Ladário da Silva [3]
Duílio Norberto Ferronatto Leite [2]
Caio Resende Martins [2]
Luciano Pessanha Moreira [1,2]

Abstract

This study investigated the mechanical behavior of thin tin-coated steel sheets (tinplate) when subjected to the Single-Point Incremental Forming (SPIF) process. Tensile tests were performed at 0°, 45°, and 90° with respect to the rolling direction to determine the anisotropic behavior of the material. SPIF tests were carried out using hemispherical tools with radii of 2.5 mm, 5.0 mm, 7.5 mm, and 10 mm. For each tool, the maximum forming angle was experimentally determined through an iterative approach while maintaining a constant target surface roughness. The results show that smaller tool radii lead to higher forming angles (up to 54°), although they require longer forming times. The limiting strains considerably exceeded those obtained in the uniaxial tensile test, with the maximum strain reaching 52%. The thickness reduction was consistent with the strain measurements, and surface roughness was evaluated using microscopy. The study highlighted the influence of tool geometry on formability, surface quality, and final geometry, providing insights for optimizing SPIF parameters in tinplate sheet applications.

Keywords: Incremental forming; SPIF; Tinplate; Surface roughness.

1 Introduction

The single-point incremental forming (SPIF) process, in its common configuration, involves the plastic deformation of thin metal sheets using a hemispherical-tipped tool. As shown schematically in Figure 1, the sheet is clamped between upper and lower supports, allowing the forming tool access to its central region. The tool performs both translational (tool path) and rotational movements (spindle speed). As a dieless forming method, SPIF offers high customization capability and low implementation costs compared to conventional stamping processes. Its applications include the production of spare parts, customized biomechanical components, small-batch manufacturing, and rapid prototyping. Some disadvantages of SPIF, such as limited dimensional accuracy and low production cadence, have been significantly mitigated through the integration of data-driven approaches, including neural networks, 3D model reconstruction, and machine vision [1].

SPIF demonstrates superior formability compared to traditional forming methods, such as stamping. Numerous analytical, numerical and experimental studies have been conducted to investigate its mechanics [2]. Martins et al. [3] reported that experimental assessments of forming limits in SPIF resulted in higher values on the forming limit curve (FLC) than those observed in conventional processes. While necking is typically considered the limiting criterion in both cases, studies evaluating sheet thickness variation with depth for various geometries have shown that plastic deformation in SPIF occurs primarily through uniform thinning until fracture, with no evidence of localized necking.

Several process parameters significantly affect surface finish and formability. According to McAnulty et al. [4], the most widely studied parameters for SPIF optimization include tool diameter, depth increment, sheet thickness, tool rotation speed, and translation speed. SPIF is predominantly applied to thin sheets of ductile materials with low yield strength, such as aluminum alloys, which require lower forming forces than steels [5]. Hussain et al. [6] experimentally assessed formability in SPIF for AA2024, AA3003, AA1060-H24, and AA2024-T4 alloys based on maximum forming angle and thickness reduction. Raju and Narayanan [7] studied the process using a commercial copper alloy sheet of 0.4 mm thickness. Other researchers, such as Centeno et al. [8], investigated the forming limits and forces in AISI 304 stainless steel (0.8 mm thick), while [9,10] applied SPIF

[1]*Programa de Pós-graduação em Engenharia Metalúrgica, Universidade Federal Fluminense, Volta Redonda, RJ, Brasil.*
[2]*Departamento de Engenharia Mecânica, Universidade Federal Fluminense, Volta Redonda, RJ, Brasil.*
[3]*Departamento de Física do ICEx, Universidade Federal Fluminense, Volta Redonda, RJ, Brasil.*

**Corresponding author:* rafaeloliveirasantos@id.uff.br
E-mails: vi_ramos@id.uff.br; ladariosilva@id.uff.br; duferronatto@id.uff.br; caiorm@id.uff.br, luciano_moreira@id.uff.br

to titanium sheets for cranial implant fabrication. Studies by [11-13] extended SPIF to polymeric sheets, and more recently has been investigated in composite materials [14].

In the present study, the mechanical behavior of tin-coated carbon steel sheets (tinplate) with a nominal thickness of 0.19 mm was experimentally investigated using the SPIF process.

Although tinplate is also used in the white goods and automotive sectors, its primary application lies in the packaging industry for the storage of paints, adhesives, aerosols, and food products.

2 Materials and methods

2.1 Material properties

In this study, the material used was tinplate with a nominal thickness of 0.19 mm. The material was tested in aged conditions. The mechanical properties of the tinplate were determined through uniaxial tensile tests. To evaluate the material's anisotropic plastic behavior, tests were conducted at 0°, 45°, and 90° relative to the sheet rolling direction (RD) using a nominal crosshead speed of 3 mm/min (10^{-3} s^{-1}). The experiments were performed using an EMIC DL2000 universal testing machine equipped with a 20 kN load cell and a contact extensometer with a 50 mm gauge length. The specimens were prepared in accordance with the ASTM E8 standard [15]. The specimens were machined on a CNC machining center with abundant coolant to prevent thermal effects.

2.2 SPIF test preparation

There are several methods to produce incremental deformation in metal sheets, making it a highly versatile process. The SPIF process was employed using a ROMI D800 CNC vertical machining center. A dedicated structure was fabricated to hold the sheet on the machining table during forming, as shown in Figure 2a. This fixture enables tool

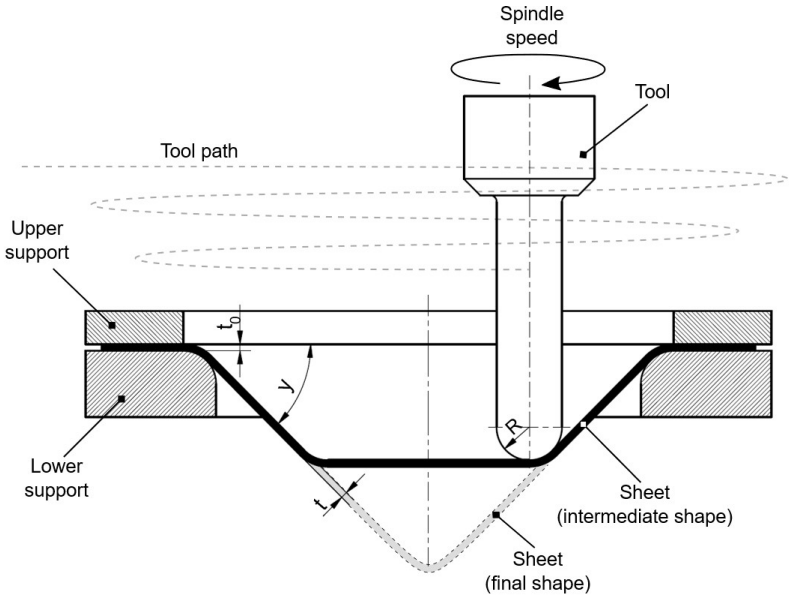

Figure 1. Schematic representation of SPIF process, adapted from Martins et al. [3].

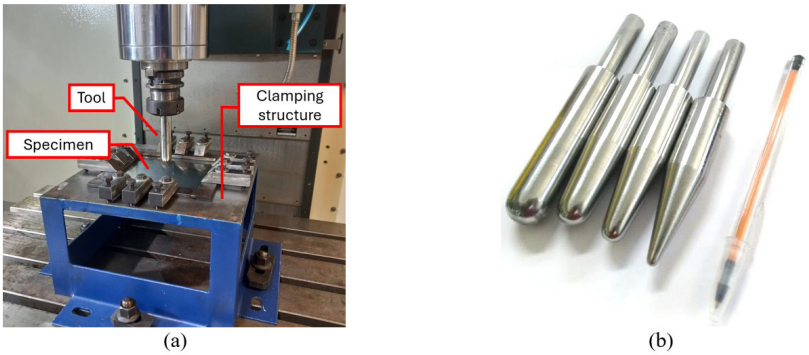

(a) (b)

Figure 2. (a) SPIF tooling and (b) adopted tools with hemispherical tips, radii: 10 mm; 7.5 mm; 5 mm; 2.5 mm.

access to a central area measuring 150 mm × 150 mm. The tool radius has great influence on the superficial roughness and the sheet's incremental formability [16,17]. Based on this, four tools' radius were tested: 10 mm, 7.5 mm, 5 mm, and 2.5 mm, as presented in Figure 2b. The CNC machining center used is equipped with a Fanuc-OiM controller. A parameterized G-code program was developed to perform the incremental forming tests. The experimental procedure involved forming the sheet into a square-based pyramid. The test is considered successful when no fractures occur along the entire length of the pyramid walls. The objective is to determine the maximum forming angle (ψ) for the given set of parameters.

The program input variables are the tool radius (R), target roughness (R_a), and tool path feed rate (f). From these inputs, the horizontal (Δx) and vertical (Δz) displacement increments were calculated according to Equation 1 and 2.

Figure 3a shows a simplified approach aimed at standardizing the surface quality regardless of the forming angle. In this procedure, the displacement increments are defined in order to maintain a constant target roughness.

$$\Delta x = \Delta z / \tan(\psi) \tag{1}$$

$$\Delta z = \sin(\psi)\sqrt{(8\,R_a R) - (4\,R_a^2)} \tag{2}$$

In this test, the tool's rotational speed is synchronized with the translational feed rate to minimize relative motion (sliding) at the tool-sheet interface. Figure 3b presents a schematic of the tool tip's contact region, illustrating the parameters used to define the spindle speed (n). Despite being referred to as a "single point" process, the actual contact occurs over a fine region extending from point "a" to point "b". The peripheral speed is zero at point "a" (center of the tool) and maximum at point "b", located at the distance equal to the radius (r). Equation 3

Provides the relationship for calculating the tool's rotational speed as a function of the translational feed rate, tool tip radius and forming angle.

$$n = \frac{f}{2\pi R \sin(\psi)} \tag{3}$$

For the SPIF test, the tool path feed rate was fixed at 500 mm/min and the target roughness at 0.008 mm (8 µm). The tool radius was updated in the program according to the tool in use, while the forming angle was determined through an iterative trial-and-error procedure. An initial forming angle was selected, and after each test, the sheet was inspected for fracture. If no fracture occurred, the forming angle was increased; otherwise, it was decreased according to a bisection algorithm until the limiting forming angle was identified.

The samples used in the SPIF test had a square geometry of 200 mm × 200 mm. To measure the deformation after forming, a standard checkered grid with 5 mm spacing was applied. An initial attempt was made to use the traditional electrolytic etching; however, due to the small thickness of the tinplate, this method negatively affected the sheet's formability by creating preferential sites for fracture. As an alternative, a CNC pen-plotter was employed to mark the grid using permanent ink.

The grid was applied to the surface opposite the one in contact with the forming tool. A thin layer of ISO 68 lubricating oil was applied to the tool-sheet contact surface to minimize friction.

2.3 SPIF evaluation

The square-based pyramidal geometry was selected for two main reasons. First, it provides a flat surface, which facilitates the strain and roughness measurements. Second, it induces a deformation mode that closely approximates plane strain, the most critical condition in the forming limit curve. Under this deformation mode, the grid deforms primarily

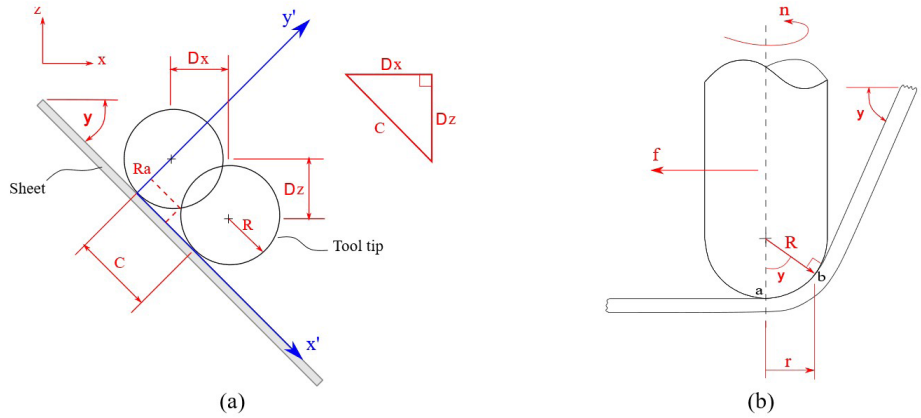

Figure 3. (a) Targeted roughness and (b) rotation synchronized with feed rate, both as functions of the prescribed forming angle and tool radius.

Table 1. Maximum forming angle (ψ) and total incremental forming time (t_t)

Radius	2.5 mm	5.0 mm	7.5 mm	10.0 mm
ψ	54.0°	48.5°	46.5°	45°
t_t	175 min	108 min	83 min	66 min

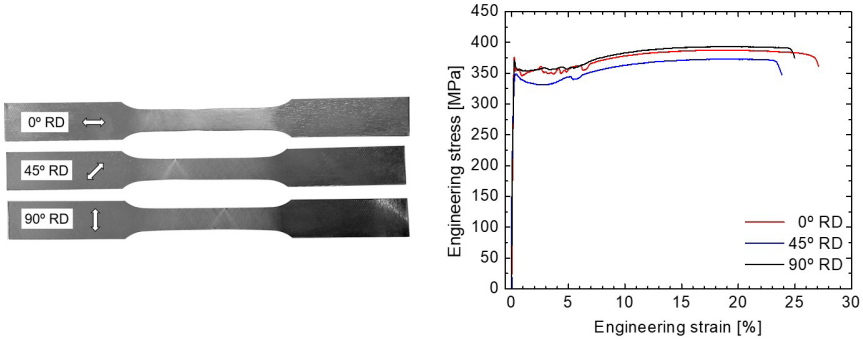

Figure 4. Uniaxial tensile test: (a) tested specimens and (b) engineering stress-strain curve, at 0°, 45°, and 90° according to the sheet rolling direction.

in one in-plane direction. In other words, assuming volume conservation during plastic deformation, if deformation occurs in only one direction in the plane, then there is a reduction in thickness equivalent to this deformation. Accordingly, in addition to measuring strain in the flat region of the sheet, the thickness along the wall of the deformed shape was also measured. The samples were sectioned along the mid-plane and measured using a micrometer of 0.01 mm precision.

To quantify the strain, the previously applied grid served as a reference. After the incremental forming process, the deformed grid was evaluated by the ASAME digital image correlation software, which provides the strain fields obtained. Surface quality resulting from the SPIF process was assessed using a Leica DCM3D confocal microscope. Measurements were conducted on sample sections oriented at 0° and 90° relative to the sheet rolling direction, for each tool radius investigated. This procedure enabled a comparative analysis of the influence of tool radius and sheet orientation on the final surface roughness at the tool-sheet interface.

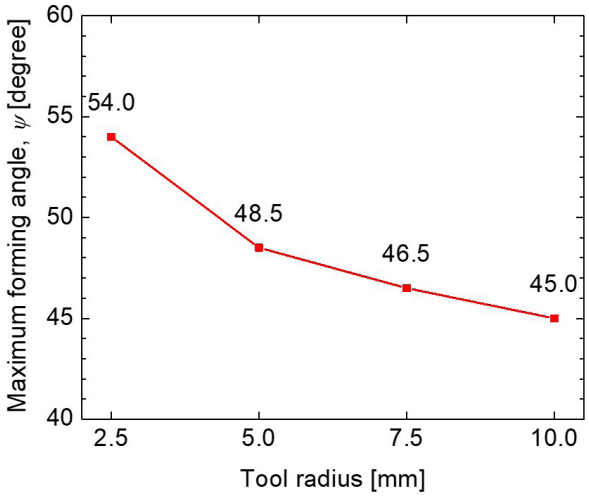

Figure 5. Influence of tool radius on maximum incremental forming angle.

3 Results

3.1 Mechanical properties

Figure 4 shows the results obtained from uniaxial tensile tests. The tinplate sheet exhibited a yield strength of 355 MPa and an ultimate tensile strength of 390 MPa at 0° RD. The yield plateau extended for about 7% strain in all three directions analyzed. Under uniaxial tension, the material presented a total elongation of 25% before the onset of fracture.

3.2 Maximum forming angle

After the iterative experimental procedure to determine the maximum forming angle for each tool radius, it was observed that reducing the tool radius increases the maximum achievable forming angle.

For the smallest tool radius of 2.5 mm, a maximum forming angle of 54° was achieved, whereas for the largest tool radius of 10 mm, the maximum angle was limited to 45° (Figure 5). According to the procedure adopted, the vertical displacement increment is automatically adjusted for each tool radius to maintain a constant target surface roughness, aiming to achieve a consistent surface finish across all tests.

However, other aspects of the process were also evaluated. Table 1 presents the total forming time required for each tool radius. Although the 2.5 mm radius tool exhibited the highest forming capability, it also resulted in a significantly longer forming time, approximately 2.6× longer compared

to the 10 mm radius tool. Even when considering the same forming angle (45°) for both tools, the forming time with the 2.5 mm radius was still 2.2× longer (146 minutes) than the 10 mm radius tool.

Figure 6 shows the SPIF test samples formed at the maximum forming angle determined for each tool radius. An important observation regarding the final geometry of the stamped parts is the influence of the tool radius on the sharpness corner. Smaller sharper corners contribute to greater dimensional stability of the sheet during forming, which is particularly relevant for thin material such as tinplate. During the SPIF test the 10 mm tool, a partial loss of geometric stability was detected, evidenced by irregular noises associated with the tool path. Additionally, the use of synchronized tool rotation with the tool path to reduce friction proved beneficial. This strategy helped prevent typical geometric distortions caused by friction between the tool and the sheet, which are often observed in SPIF process where the tool surface has a relative velocity in contact with the sheet.

3.3 Limiting strains and thickness reduction

After determining the maximum forming angle as a function of tool radii, three replicate tests were performed to confirm the absence of fracture. Figure 7 presents the average values of the limiting strains (major and minor in-plane principal strains) measured on the wall of the samples at 0° and 90° RD. The minor strain values are close to zero, while the major strain values are positive, indicating a deformation mode very close to plane strain, which represents a critical condition in the forming limit diagram (FLD). These results highlight the capability of incremental forming to achieve limiting strains significantly higher than those obtained in conventional forming processes, even for tinplate sheets. For all tool radii tested, the major strain exceeded the value observed in the uniaxial tensile test (approximately 25%), ranging from 34% to 52% for the tools with a radius of 10 mm and 2.5 mm, respectively.

Figure 8 presents the results of the sheet thickness measurements. The final thickness obtained for the tool with a 2.5 mm radius was approximately (0.119 ± 0.003) mm, corresponding to a thickness strain of 48%. For the tool with a 10 mm radius, the final thickness was (0.140 ± 0.002) mm, equivalent to a thickness strain of 31%.

3.4 Tinplate surface roughness

The tinplate sheet used in this study features a stone-finish coating. The three most common types of surface finishes are

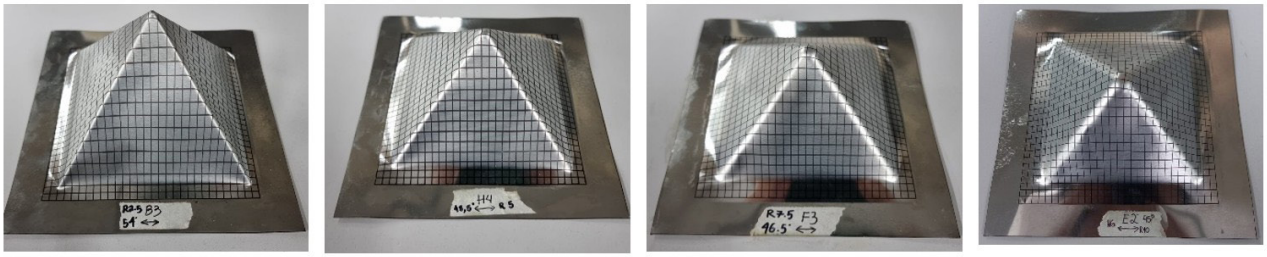

Figure 6. Formed sheets after SPIF test using the following tool radius: (a) 2.5 mm, (b) 5 mm, (c) 7.5 mm, and (d) 10 mm.

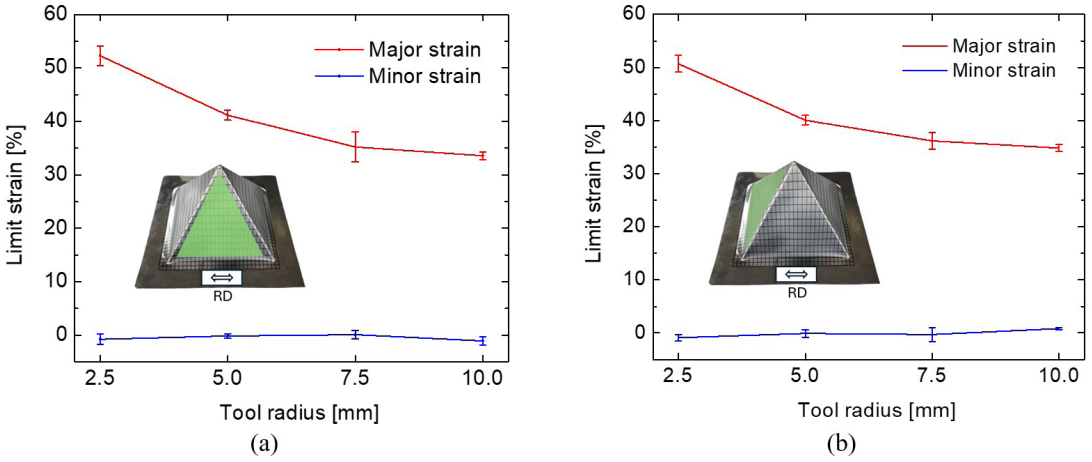

Figure 7. Major and minor strains measured on specimen wall: (a) 0° and (b) 90° RD.

bright, matte, and stone finishes, the latter providing a bright appearance with fine linear textures. A sample in the as-received condition was analyzed using a confocal microscope, and the initial surface roughness was measured at (0.49 ± 0.01) µm. Figure 9a shows the profile of one of the scanned lines used to calculate the sheet roughness, while Figure 9b presents a topographic image of the sample, where the characteristic fine lines of the stone finish can be clearly observed.

Figure 10 presents the roughness of the surface values of the sheet under two different conditions. In the first case, Figure 10a, the forming angle was kept constant at 45°, while only the tool radius was varied. In the second case, Figure 10b, both tool radius and maximum forming angle (specific to each tool radius) were varied. The results show that tools with smaller radii tend to produce smoother surfaces. In the case of the tinplate, roughness measured

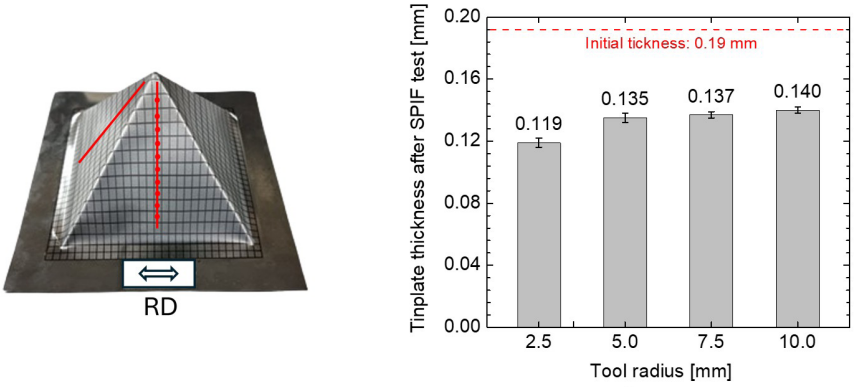

(a) (b)

Figure 8. Final thickness of the tested sheet: (a) measured points and (b) average values.

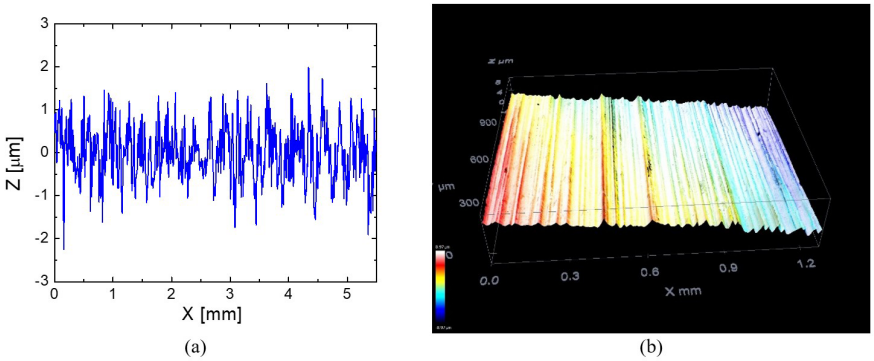

(a) (b)

Figure 9. (a) Surface roughness profile and (b) topography of tinplate in the as-received condition.

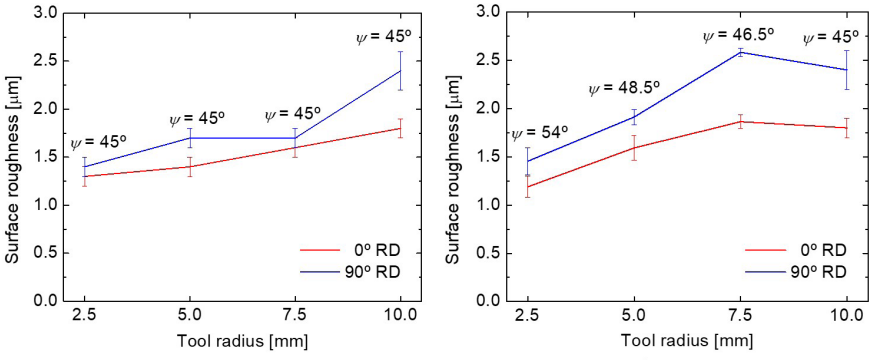

(a) (b)

Figure 10. Surface roughness for (a) different tool radius with the same forming angle (45°) and (b) different tool radius at their respective maximum forming angles.

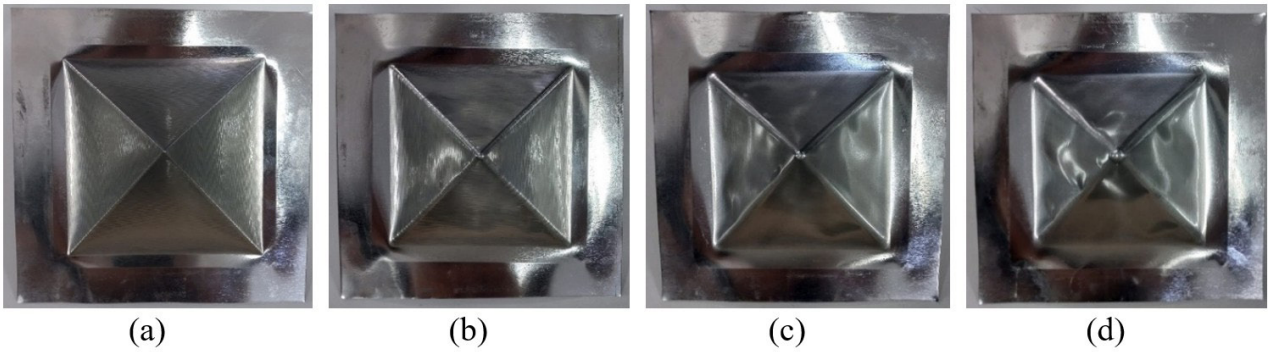

Figure 11. Specimens' inner surfaces for radius: (a) 2.5 mm, (b) 5 mm, (c) 7.5 mm, and (d) 10 mm.

at 90° RD (and the orientation of the stone-finish coating) exhibited higher values for all tool radii.

Figure 11 shows the inner surface of the specimens after the SPIF process. For tools with lager radius (10 mm), the surface appeared wavy, resembling localized wrinkling.

In contrast, tools with smaller radius (2.5 mm) produced flatter surfaces, although a distinct surface texture pattern was still observed.

4 Conclusion

In this work, a tinplate with a thickness of 0.19 mm was experimentally subjected to the incremental forming by the SPIF process using pyramidal geometry and different tool radii. The experimental investigation confirmed that the SPIF process can significantly enhance the formability of tinplate sheets compared to conventional forming methods. Smaller tool radius led to higher forming angles and greater in-plane and thickness trains, albeit with increased processing times. Surface roughness was influenced by tool radius and sheet orientation, with smaller tools yielding better surface finishes. These findings underscore the potential of SPIF for fabricating customized thin-walled components using tinplate, particularly when high geometric precision and surface quality are required.

Acknowledgements

The authors greatly acknowledge CSN (Companhia Siderúrgica Nacional) for supplying the tinplate sheets. The authors would also like to thank the laboratories of Applied Mechanics (EEIMVR), Materials Characterization (LMCM-ICEx), PROPPI/UFF, and the Graduate Program in Metallurgiy at UFF (PPGEM), for the support and infrastructure.

References

1 Kumar SP, Stanley VJ, Nimesha S. Data-driven approaches in incremental forming: unravelling the path to enhanced manufacturing efficiency using data acquisition. International Journal of Lightweight Materials and Manufacture. 2025;8:165-181.

2 Behera AK, Sousa RA, Ingarao G, Oleksik V. Single point incremental forming: an assessment of the progress and technology trends from 2005 to 2015. Journal of Manufacturing Processes. 2017;27:37-62. https://doi.org/10.1016/j.jmapro.2017.03.014.

3 Martins PA, Bay N, Skjoedt M, Silva MB. Theory of single point incremental forming. CIRP Annals. 2008;57(1):247-252. https://doi.org/10.1016/j.cirp.2008.03.047.

4 McAnulty T, Jeswiet J, Doolan M. Formability in single point incremental forming: a comparative analysis of the state of the art. CIRP Journal of Manufacturing Science and Technology. 2017;16:43-54. https://doi.org/10.1016/j.cirpj.2016.07.003.

5 Jeswiet J, Macari F, Hirt G, Bramley A, Duflou J, Allwood J. Asymmetric single point incremental forming of sheet metal. CIRP Annals. 2005;54(2):88-114. https://doi.org/10.1016/S0007-8506(07)60021-3.

6 Hussain G, Hayat N, Gao L. An experimental study on the effect of thinning band on the sheet formability in negative incremental forming. International Journal of Machine Tools & Manufacture. 2008;48(10):1170-1178. https://doi.org/10.1016/j.ijmachtools.2008.02.003.

7 Raju C, Narayanan C. Application of a hybrid optimization technique in a multiple sheet single point incremental forming process. Measurement: Journal of the International Measurement Confederation. 2016;78:296-308. https://doi.org/10.1016/j.measurement.2015.10.025.

8 Centeno G, Bagudanch I, Martínez-Donaire AJ, Garcia-Romeu ML, Vallellano C. Critical analysis of necking and fracture limits and forming forces in single point incremental forming. Materials & Design. 2014;63:20-29. https://doi.org/10.1016/j.matdes.2014.05.066.

9 Castelan J, Schaeffer L, Daleffe A, Fritzen D, Salvaro V, Da Silva FP. Manufacture of custom-made cranial implants from DICOM images using 3D printing, CAD/CAM technology and incremental sheet forming. Revista Brasileira de Engenharia Biomédica. 2014;30(3):265-273. https://doi.org/10.1590/rbeb.2014.024.

10 Sharma A, Shrivastava P, Nagargoje A, Mulay A. Multiscale residual stress analysis and microstructure characterization of Ti-grade 2 implant fabricated by adaptive tool path-driven SPIF process. Materials Characterization. 2025;222:114861. https://doi.org/10.1016/j.matchar.2025.114861.

11 Davarpanah MA, Mirkouei A, Yu X, Molhotra R. Effects of incremental depth and tool rotation on failure modes and microstructural properties in single point incremental forming of polymers. Journal of Materials Processing Technology. 2015;222:287-300. https://doi.org/10.1016/j.jmatprotec.2015.03.014.

12 Bagudanch I, Centeno G, Vallellano C, Garcia-Romeu ML. Revisiting formability and failure of polymeric sheets deformed by single point incremental forming. Polymer Degradation & Stability. 2017;144:366-377. https://doi.org/10.1016/j.polymdegradstab.2017.08.021.

13 Durante M, Formisano A, Lambiase F. Incremental forming of polycarbonate sheets. Journal of Materials Processing Technology. 2018;253:57-63. https://doi.org/10.1016/j.jmatprotec.2017.11.005.

14 Hussain G, Hassan M, Wei H, Buhl J, Xiao M, Iqbal A, et al. Advances on Incremental forming of composite materials. Alexandria Engineering Journal. 2023;79:308-336. https://doi.org/10.1016/j.aej.2023.07.045.

15 ASTM International. ASTM E8/E8M: Standard test method for tension test of metallic materials. West Conshohocken (PA): ASTM International; 2013.

16 Al-Ghamdi KA, Hussain G. Threshold tool-radius condition maximizing the formability in SPIF considering a variety of materials: experimental and FE investigations. International Journal of Machine Tools & Manufacture. 2015;88:82-94. https://doi.org/10.1016/j.ijmachtools.2014.09.005.

17 Bishnoi P, Chandna P. Optimizing the SPIF parameters for enhancing microhardness and surface quality in Inconel 625 superalloy components. Journal of Alloys and Compounds. 2024;997:174839. https://doi.org/10.1016/j.jallcom.2024.174839.

Received: 8 Oct 2025
Accepted: 2 Dec 2025

Editor-in-charge:
André Luiz Vasconcellos da Costa e Silva